Behaviour & Information Technology, 2014
Vol. 33, No. 9, 892–904, http://dx.doi.org/10.1080/0144929X.2013.819937

Taylor & Francis
Taylor & Francis Group

Personalised and dynamic image precompensation for computer users with ocular aberrations

Jian Huang*, Armando Barreto, Peng Ren and Malek Adjouadi

Department of Electrical and Computer Engineering, Florida International University, Miami, FL, USA

(*Received 15 January 2013; accepted 24 June 2013*)

Most of the computer users with ocular aberrations such as myopia, hyperopia and other high-order aberrations are subject to visual blurring, which may impede the efficient interactions with the computers. Conventional methods used to counter visual blurring include spectacles and contact lenses. In this paper, we introduce an image preprocessing method that is designed to counteract the visual blurring caused by the aberration of the eye. In this method, the presented images are preprocessed by performing personalised compensation according to the ocular aberration of the computer user. In order to overcome the mismatch between the aberration used to generate the precompensation and the actual aberrations at the time of viewing, dynamic ocular aberrations are derived from the resizing of the initial aberration data measured by the wavefront analyzer. The dynamic ocular aberrations are used to update the image precompensation in real time. Results of human subject experiment show that the image recognition accuracy was significantly increased after the dynamic precompensation was applied. Subjective impressions from the participants confirmed the effectiveness of the method.

Keywords: personalised precompensation; user modelling; image enhancement; ocular aberration; visual blurring; Zernike polynomials; wavefront aberration resizing

1. Introduction

People with ocular aberrations suffer from various visual problems in their daily activities. Without considering the neural processing of the retinal image, visual acuity is reduced due to the ocular aberrations existing in the human eyes. In the context of computer use, the visual blurring caused by ocular aberrations impedes the efficient interaction between the computer and its user. Thus, people with ocular aberrations may encounter difficulties in the recognition of icons, menus and other pictorial presentations, which limit their ability to search and access correct information.

Generally, visual quality is mostly degraded by the low-order aberrations (e.g. myopia, hyperopia and astigmatism). Approximately 25% of American adults are myopic and require some form of correction to see clearly beyond an arm's length (Leonard 2001, Vitale *et al.* 2009). It is also reported that refractive errors affect approximately one-third of persons 40 years or older in the USA and Western Europe, and one-fifth of Australians (The Eye Diseases Prevalence Research Group 2004). Traditionally, ocular aberrations are corrected by spectacles or contact lenses. More recently, refractive surgeries (e.g. laser-assisted in situ keratomileusis (LASIK)) have also become a popular alternative, by reshaping the cornea using a laser (Dai 2008). These correction methods work well in most cases. However, for some people with visual impairments (e.g. cataracts, glaucoma, macular degeneration) (Munoz *et al.* 2000), low vision problems still exist even when spectacles or contact lenses are used. In addition, these methods are generally only used to correct low-order aberrations and not effective for high-order aberrations (Liang *et al.* 1997). In fact, it was not practical to measure the accurate aberrations of the human eyes until the appearance of the Shack–Hartmann wavefront sensor (Liang and Williams 1997). After that, adaptive optics techniques have been used to correct high-order aberrations of the human eyes for more visual benefits (Liang *et al.* 1997, Fernández *et al.* 2001, Roorda 2011). The effects of high-order aberrations were evaluated through standard vision tests (e.g. visual acuity and contrast sensitivity) and also natural images in daily activities (e.g. familiar faces) (Guirao *et al.* 2002, Sawides *et al.* 2010). However, owing to the high cost and physical size limitations of the adaptive optics system, instruments based on it are not practical to be used for daily activity purposes at present. Therefore, it is still meaningful to seek new approaches to address the problem of ocular aberration correction in more flexible and efficient ways.

Image enhancement techniques have been widely used to improve low-quality images in order to make them more suitable to be viewed in different applications (Gonzalez and Woods 2002). General image enhancement techniques usually seek to optimise certain desired features (e.g. high-frequency information, histogram distribution) to improve details or contrast. Under most circumstances, the performance or effects of these methods are assessed with the

*Corresponding author. Email: jhuan004@fiu.edu

© 2013 Taylor & Francis

assumption that the image viewers have normal vision. In fact, images can be preprocessed in terms of the specific user's visual characteristics and preferences before presenting them on the screen. Taking advantage of the computer's processing ability, it is possible to prefilter the images and enhance the visual performance of the users without normal vision. So far, several image enhancement methods have been developed to help patients with low vision, even though the studies and applications in this area are still relatively quite few. Initially, Peli (1984) introduced an adaptive enhancement method, in which the high-frequency information in a specific range was enhanced based on the knowledge of the contrast sensitivity loss of the visually impaired subjects. In subsequent studies, this method was used to improve the text reading (Fine and Peli 1995) and face recognition ability (Peli *et al.* 1994). By using similar methods, Lawton (Lawton 1992, Lawton *et al.* 1998) reported that the reading speed of age-related macular degeneration patients was significantly faster with the enhancement of customised filters according to the normalised contrast sensitivity function (CSF). Other methods attempted to raise the visual quality by highlighting or strengthening the edge information, with the purpose of enhancing the local contrast of images (Peli *et al.* 2004, Leat *et al.* 2005, Wolffsohn *et al.* 2007). Tang *et al.* (2004) proposed an enhancement method for JPEG images for low vision viewers, in which the enhancement is integrated in the process of compression. Enhancement techniques for video images were also developed to facilitate watching video, especially television, by low vision subjects (Kim *et al.* 2004, Peli 2005).

The studies introduced above mainly targeted to improve the visual performance of people with various visual impairments, but did not address the visual blurring caused by the general aberrations of the eyes. Although ocular aberrations such as myopia and hyperopia are usually not considered as diseases, uncorrected refractive errors are the most common cause of visual impairments (Leonard 2001). In fact, visual impairments are always concomitant with aberrations such as severe refractive errors. In previous studies, enhancement models were mainly developed in terms of the patient's CSF (Peli 1984, Lawton *et al.* 1998), as an approximation to the frequency perception ability of the patient's eyes. This empirical characterisation is highly sensitive to measurement parameters and does not account for the dynamic behaviour of the human eye.

This study describes a personalised and dynamic image precompensation method to improve the visual performance of the computer users with ocular aberrations, without using any external correction devices such as spectacles or contact lenses. In this method, images presented to the viewer are compensated in advance, aiming to counteract the visual blurring caused by the ocular aberrations. Pupil size variations, primarily caused by the changes of illumination at the time of viewing, have considerable impact on the aberration of the eye. Thus, in order to improve the performance achieved by applying static precompensation (Alonso *et al.* 2005), the precompensation model needs to be adjusted dynamically along with the real-time pupil sizes of the user. In this study, we collected the pupil data through an eye tracking system integrated with the computer monitor, for resizing and updating the ocular aberrations.

2. Background

2.1. Ocular aberration

The visual system is the combination of the optical system of the eye and the neural processing of the light that reaches the retina (Thibos 2000). The former part can be characterised by the wavefront of light travelling to the retina. Based on the wave optics theory, ocular aberration is defined as the difference between the actual aberrated wavefront of the eye and an ideal spherical wavefront. All human eyes have some degree of aberration and any ocular aberration will produce degradation on the resulting retinal image, as shown in Figure 1(a).

Every human eye has unique aberrations with individualised patterns. This uniqueness occurs not only in the eyes of different people, but also in each eye of the same person. Even if a person's eyes have equal prescription of glasses or contact lenses, their actual ocular aberrations are different. In general, ocular aberrations include low-order aberrations and high-order aberrations. Low-order aberrations, such as myopia, hyperopia and astigmatism are well known. The low-order aberrations result in common visual blurring, hence contributing most of the degradation in visual perception. Generally, high-order aberrations do not degrade the

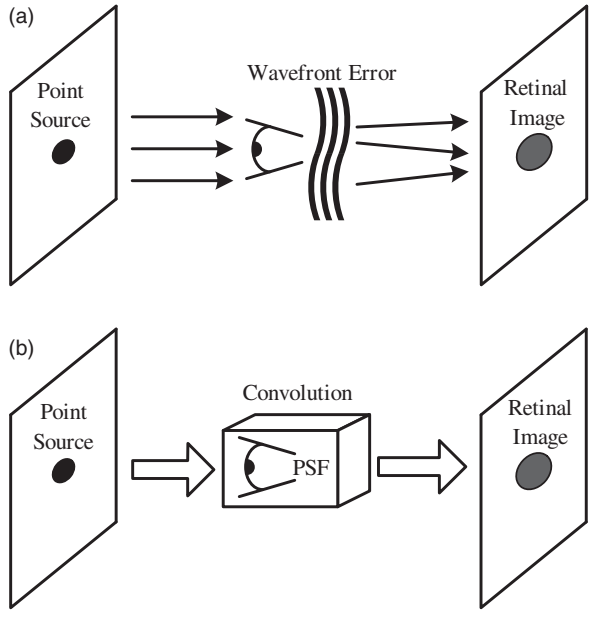

Figure 1. Retinal image formation as (a) wavefront propagation and (b) convolution process with the point spread function of the eye.

vision performance seriously. However, significant effects can be produced on the retinal image quality once the pupil becomes large, as the corresponding high-order aberrations are increased (Liang and Williams 1997). Large amounts of high-order aberrations can trigger symptoms like glare, halos, ghosts, etc.

2.2. Zernike representation of aberrations

Owing to the development of wavefront sensing technology, fast and accurate measurement of ocular aberration has become readily available. In general, the aberration data are represented as a wavefront map of errors. More specifically, the ocular aberration with pupil radius P_r is usually decomposed into a set of Zernike polynomials and coefficients as

$$W(r,\theta) = \sum_{i=0}^{\infty} a_i Z_i(\rho,\theta), \tag{1}$$

where r is the physical radial variable, $\rho = r/P_r$ is the normalised radial variable from 0 to 1 and a_i is the coefficient for the basis function $Z_i(\rho,\theta)$, which represents the corresponding Zernike polynomial in the form of polar coordinates. i is the single index of the Zernike polynomials. Zernike polynomials are orthogonal over the circular aperture.

2.3. Retinal image formation

The optical system of the human eye is mainly composed of the cornea, the iris, the pupil, the lens and the retina. However, if we consider them as a whole, the imaging process in the human eye can be described as the mapping of a viewed object to the light information on the retina according to the optics of the eye. This mapping process can be further simplified by the introduction of the point spread function (PSF), which is defined as the image of a single point source that the eye forms on the retina. Once we know the wavefront aberration of the eye, its PSF can be calculated by using the Fraunhofer approximation (Goodman 2005) as

$$\mathrm{PSF}(r',\theta') = |\mathcal{F}\{A(r,\theta)\,\mathrm{e}^{-\mathrm{i}(2\pi/\lambda)W(r,\theta)}\}|, \tag{2}$$

where $\mathcal{F}$ is the Fourier transform operator, $A(r,\theta)$ is the pupil function that defines the pupil shape, size and the light transmission through the pupil, and λ is the wavelength of the light entering into the pupil.

The PSF is a very useful tool to describe the visual performance of the eye. In most cases, any object viewed can be considered as a two-dimensional array of point sources. The images of these point sources are diffused by the PSF and superimposed, forming the retinal image of the object. Thus, the retinal image formation of an object can be described as the convolution of the intensities of the object and the PSF of the eye, as shown in Figure 1(b).

3. Methods

Image is one of the most fundamental elements to present information used by modern graphic interfaces. For computer users with normal vision, the perception of images displayed (e.g. pictures and icons) is accomplished with satisfactory clearness and sharpness, as the images are designed and rendered with careful consideration. However, these well-designed images may not be fit for those people without normal vision. Limited by their vision ability, many computer users with severe ocular aberrations may encounter difficulties in identifying images, thereby hindering their further access to computer resources. Thus, to overcome the visual degradation caused by the aberrations, the images can be designed in particular ways with specific compensation performed on the original images before presenting.

The image precompensation problem introduced here has similarities with non-blind image restoration. In general, the image restoration process assumes that the degradation model is known or can be estimated in reliable ways. Similarly, for image precompensation, the visual degradation model (PSF of the eye) of the specific observer is required as a priori knowledge before the customised compensation can be produced. On the other hand, image precompensation is substantially different from image restoration. Image restoration methods post-process the degraded image based on the known degradation information in order to restore the original image from its degraded version, whereas the image precompensation method modifies the original images in a particular pattern, for neutralising the visual blurring caused by the aberration. Image restoration is a relatively mature research field with a long history. So far, numerous image restoration techniques have been developed to recover the images from degradation with different assumptions for the prior knowledge. The prior knowledge includes knowledge of the degradation, statistical information of the noise and the original image, etc. Usually, the process of image restoration will be greatly facilitated and simplified if the complete degradation model is known. Compared with image restoration, image precompensation is subject to some new problems and difficulties due to its specificity. One big challenge is that the image perceived by the user is not accessible. Thus, classical image restoration methods that involve iterative optimisation (Richardson 1972, Katsaggelos *et al.* 1991, Rudin *et al.* 1992) are not applicable here due to the lack of reliable ways to update the estimation for convergence. In this study, we use the inverse Wiener filter to produce the personalised compensation, since a relatively accurate PSF can be obtained.

3.1. Inverse Wiener filtering

Let us assume that an image with intensity $o(x,y)$ is to be viewed by a computer user. Because of the aberration

existing in the user's eye, the retinal image generated is degraded, resulting in an intensity distribution $i(x,y)$. The PSF of the user's eye is defined as $\mathrm{PSF}(x,y)$, sampled with the same resolution as the image. The degradation of the image can be described as a convolution process:

$$i(x,y) = o(x,y) * \mathrm{PSF}(x,y). \tag{3}$$

The optical transfer function (OTF), another useful function for describing the visual characteristics of the human eye, is derived by Fourier transform of the PSF:

$$\mathrm{OTF}(u,v) = \mathcal{F}\{\mathrm{PSF}(x,y)\}, \tag{4}$$

where u and v are the horizontal and vertical spatial frequencies, respectively, in discrete form. The modulation transfer function (MTF) is defined as the modulus of the complex-valued OTF:

$$\mathrm{MTF}(u,v) = |\mathrm{OTF}(u,v)|. \tag{5}$$

Applying Fourier transform, the degradation process is described in the frequency domain as

$$I(u,v) = O(u,v)\mathrm{OTF}(u,v). \tag{6}$$

Now, the problem is how to produce an image with appropriate compensation to replace the original image $o(x,y)$ to be presented to the viewer. One intuitive idea is using inverse filtering, in which the $O(u,v)$ is divided by $\mathrm{OTF}(u,v)$ in advance to counteract the blurring effects. However, this is not practical since the measurement error of the ocular aberrations and noise will be amplified during the inverse filtering, especially when $\mathrm{OTF}(u,v)$ is close to zero. Thus, the inverse Wiener filter is used here to produce the desired compensated image, which is calculated by

$$c(x,y) = \mathcal{F}^{-1}\left\{\frac{O(u,v)}{\mathrm{OTF}(u,v)}\frac{\mathrm{MTF}(u,v)^2}{\mathrm{MTF}(u,v)^2 + K}\right\}, \tag{7}$$

where $\mathcal{F}^{-1}$ represents inverse Fourier transform and $c(x,y)$ is the image with personalised compensation generated to replace the original image. Since no statistical information of the measurement error and noise is available, K is a small empirical constant that is used to suppress the amplification of high-frequency error.

Thus, the retinal image $p(x,y)$ when viewing the compensated image $c(x,y)$ is generated as

$$p(x,y) = c(x,y) * \mathrm{PSF}(x,y). \tag{8}$$

Two examples of this process are shown in Figure 2, in which a person with −6.8 diopter (D) spherical error is simulated to view the original images and images with precompensation, respectively, at a distance of 0.3 m. The blurring in this simulation was generated from the real aberration data of an actual subject measured by the wavefront sensor. From Figure 2, it is observed that the shapes and edges of the retinal images are much sharper after the precompensation is applied. This shows the potential of our method to relieve the visual blurring caused by ocular aberration, even though the process of precompensation also introduces some side effects. First, ringing artefacts are

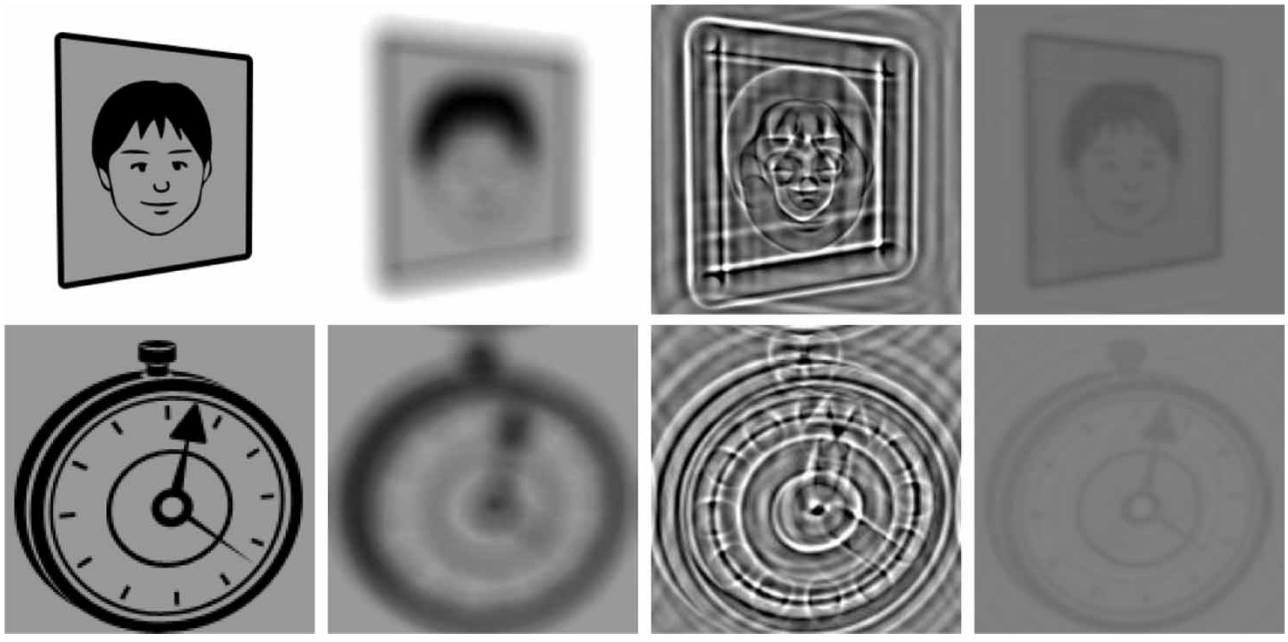

Figure 2. Simulation examples of image precompensation. Columns from left to right: original images with cartoon face and clock, blurred retinal images with −6.8 D spherical error when viewing the original images in the first column, images with precompensation, retinal images when viewing the images in the third column. In this simulation, the viewing distance was set as 0.3 m and both the measured and viewing pupil diameters were assumed to be 5.2 mm.

found around the edges of images in the right column of Figure 2. This is caused by the regularisation error in the process of inverse Wiener filtering, as a tradeoff with the suppression of the noise amplification. More importantly, we notice that the contrast is evidently reduced after the image is compensated. This problem of contrast loss will be discussed in detail next.

3.2. *Contrast loss of precompensation*

In general, the PSF of the human eyes behaves like a low-pass filter, blurring the high-frequency details of the viewed images. In comparison, the precompensation process behaves like a high-pass filter even though it does not attenuate the low-frequency components directly. While precompensation reduces the degradation caused by the eye's aberration, the compensated image usually has a wider intensity range than the original and may include negative components. One the other hand, display devices (e.g. LCD) only have limited intensity scales. Thus, the intensity values of the compensated image need to be shifted and scaled before it can be displayed. Suppose the intensity range of the compensated image $c(x,y)$ is $[c_{\min}, c_{\max}]$ and the range of the display device is $[d_{\min}, d_{\max}]$. In order to fit $c(x,y)$ in the range of display device, proportional scaling and linear shifting are performed. After that, the new image for display is given by

$$d(x,y) = \frac{(d_{\max} - d_{\min})[c(x,y) - c_{\min}]}{c_{\max} - c_{\min}} + d_{\min}. \quad (9)$$

Define α as

$$\alpha = \frac{d_{\max} - d_{\min}}{c_{\max} - c_{\min}} \quad (10)$$

and define β as

$$\beta = d_{\min} - \frac{c_{\min}(d_{\max} - d_{\min})}{c_{\max} - c_{\min}}. \quad (11)$$

Then, the new retinal image $p'(x,y)$ is predicted as

$$p'(x,y) = \alpha c(x,y) * \mathrm{PSF}(x,y) + \gamma \quad (12)$$

in which γ is a constant defined as

$$\gamma = \beta \mathrm{PSF}(x,y). \quad (13)$$

This shows that the retinal image has been compressed with a ratio determined by α. In practice, the range $[c_{\min}, c_{\max}]$ is always much wider than $[d_{\min}, d_{\max}]$. Thus, it is obvious that α is much smaller than 1. The smaller the α, more is the contrast lost. To relieve the contrast loss limitation, the contrast of compensated images is enhanced by discarding non-essential information around the two ends of the histogram and extending the range of the main histogram shape (Huang *et al.* 2012). After the enhancement, the histograms of the images in the first, third and fourth columns of Figure 2 are shown in Figure 3 from left to right, respectively. We find that the intensities of the retinal images when the compensation is applied concentrate in a narrow band near the background level even though the histograms of the compensated images have been extended towards both ends.

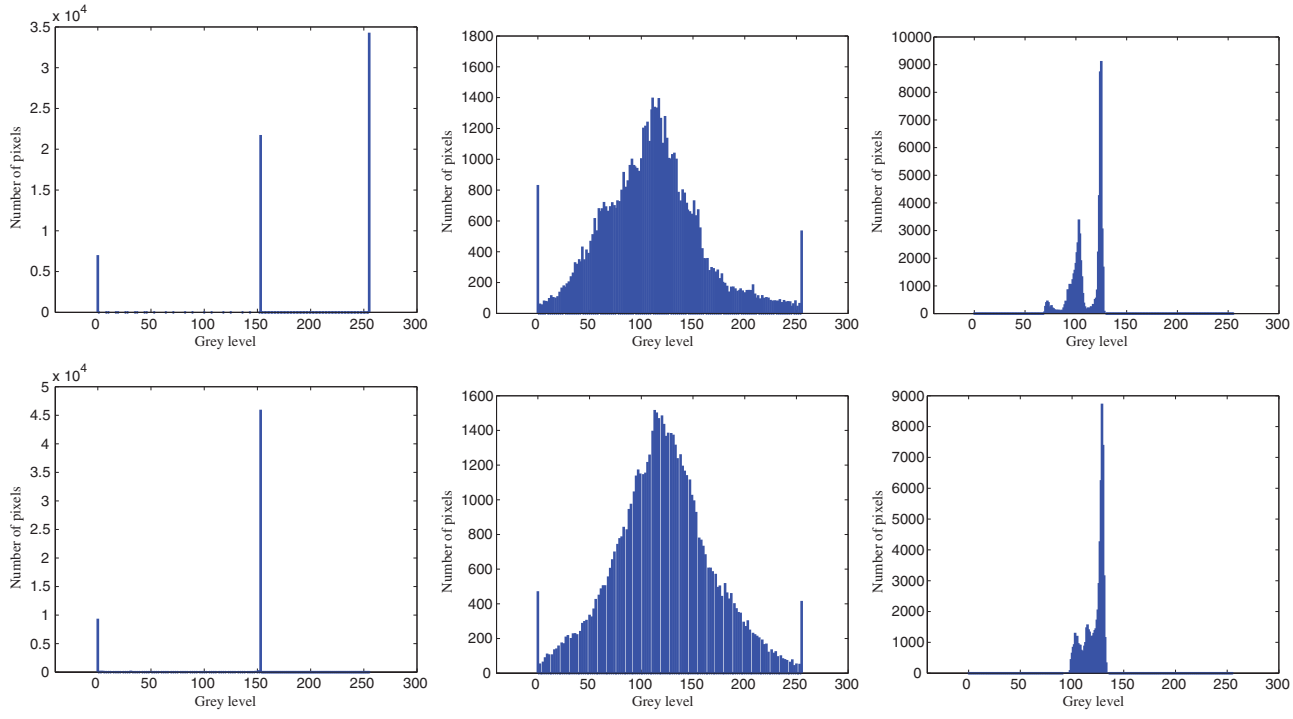

Figure 3. Left column: histograms of the images in the first column of Figure 2. Middle column: histograms of the images in the third column of Figure 2. Right column: histograms of the images in the fourth column of Figure 2.

3.3. Dynamics of ocular aberrations

The simulation results in Figure 2 are obtained with the assumption that the measured ocular aberrations are the same as the ocular aberrations at the time of viewing. This means that the simulated viewing process is implemented on the basis of a completely accurate degradation model. In practice, however, this perfect equality is not possible and the differences between them can be quite large.

As an optical system, the human eye is not static all the time. Even under steady viewing conditions, the optical characteristics of the human eye exhibit temporal instability in the form of fluctuations. The magnitude of these fluctuations is approximately 0.03–0.5 D with frequencies up to 5 Hz (Charman and Heron 1988). Traditionally, these fluctuations are characterised with low-order aberrations such as defocus and astigmatism. More recent studies (Hofer *et al.* 2001, Iskander *et al.* 2004) reported that fluctuations also exist in other high-order aberrations, though these fluctuations have no significant impact on the retinal image quality. Compared to the overall aberration, the aberration variation due to the accommodation fluctuations are very small and its impact on the visual quality is hard to notice. Thus, in this study, the fluctuations of aberration during steady viewing conditions will not be involved in the compensation.

In the context of computer use, the key factor that affects the ocular aberrations of computer users is the pupil variations. With different pupil sizes, the visual perception of the same eye can be altered considerably. So far, many factors are believed to be able to cause changes of pupil size, including physiological, psychological and emotional stimuli (Winn *et al.* 1994, Muma *et al.* 2010). In spite of this, the short-term pupil variations are primarily triggered by the changes of the illumination conditions. One well-known fact is that the pupil dilates as the ambient becomes darker and constricts as the ambient becomes brighter. Thus, static compensation will become problematic if the measured aberration data are used without update. Considering that we always measure the aberration data under a relatively dark condition, the actual aberration at the time of viewing will be different from the original one, measured by the wavefront analyzer.

As the image precompensation largely depends on the accuracy of the precompensation model, its performance will be deteriorated if mismatched aberration data are used to produce the compensation. Figure 4 shows the simulation results when the eye assumed in Figure 2 views the compensated images that are generated based on the original measured aberration with several smaller viewing pupil sizes. It is found that as the viewing pupil size increases towards the measured pupil size, the quality of the retinal images gets better. When the pupil diameter increases to 5.0 mm, the retinal image becomes close to the retinal images obtained with the matched pupil size (5.2 mm).

3.4. Resizing of ocular aberration

The pupil variations in realistic scenarios of computer use require us to update the ocular aberration that is used to produce the compensation. Thus, it is necessary to find a reliable and accurate method to resize the wavefront aberration measured with a specific pupil size to new sizes. As

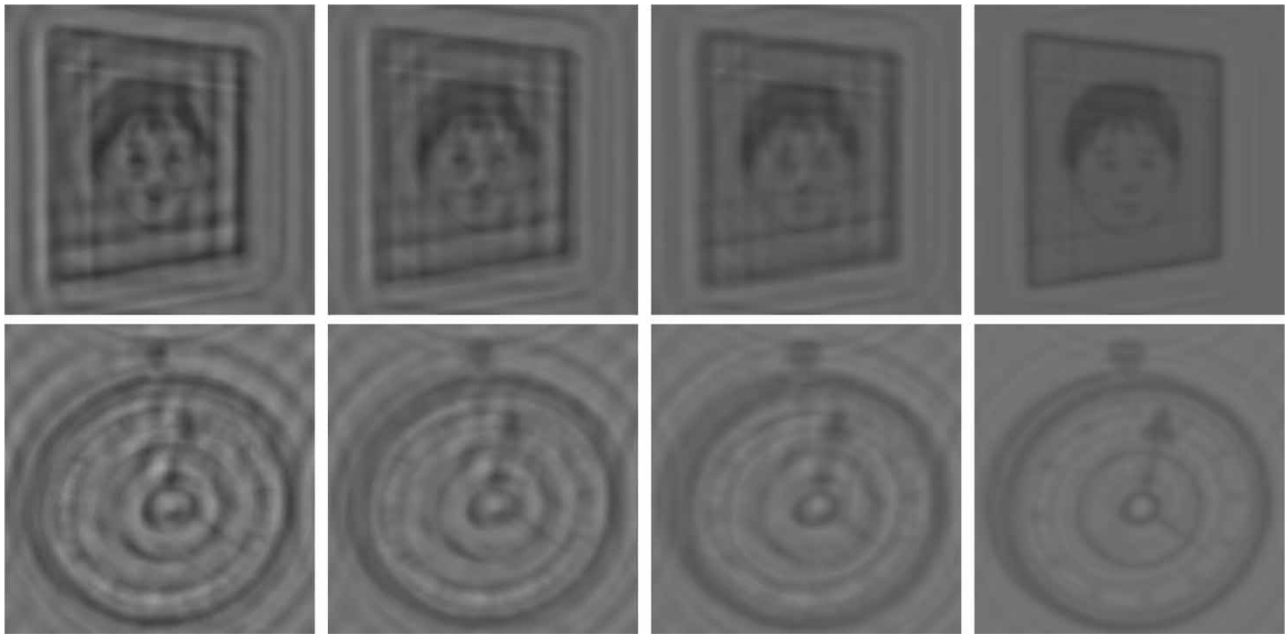

Figure 4. Retinal images when viewing the compensated images in the third column of Figure 2 by constricted pupil with diameters 3.5, 4.0, 4.5 and 5.0 mm from left to right. Note that the compensated images here are generated based on the initial aberration with 5.2 mm pupil diameter.

we introduced before, the initial ocular aberration data measured by wavefront sensors is usually reported as a set of Zernike coefficients. Due to the orthogonality of the Zernike polynomials, the Zernike coefficients are associated with a specific pupil diameter. For the same wavefront aberration map, the Zernike coefficients will be different if different pupil sizes are assigned. Thus, the problem becomes how to derive the new coefficients associated with a new pupil size from the original coefficients.

The Zernike polynomials are composed of three components: normalisation component, radial component and azimuthal component. For computing convenience, Zernike polynomials are defined in a double indexing scheme as

$$Z_n^m(r,\theta) = N_n^m R_n^{|m|}(r) M(m,\theta), \tag{14}$$

where r is the physical radial variable and θ is the polar angle. The normalisation component is defined as

$$N_n^m = \sqrt{\frac{2(n+1)}{1+\delta_{m0}}}, \tag{15}$$

where δ_{m0} is the delta function that has the value of 1 when $m = 0$ and 0 when $m \neq 0$. The radial function is defined as

$$R_n^{|m|}(r) = \sum_{s=0}^{0.5(n-|m|)} \frac{(-1)^s (n-s)! r^{n-2s}}{s![0.5(n+|m|)-s]![0.5(n-|m|)-s]!} \tag{16}$$

and the azimuthal function is defined as

$$M(m,\theta) = \begin{cases} \cos(m\theta) & \text{for } m \geq 0, \\ -\sin(m\theta) & \text{for } m < 0. \end{cases} \tag{17}$$

In the equations above, n is the order of the Zernike polynomials. For a given order n, m can only take on values of $-n, -n+2 \cdots n-2, n$. With the double indexing scheme, the ocular aberration with pupil radius P_r can be reconstructed by

$$W(r,\theta) = \sum a_n^m Z_n^m(\rho,\theta), \tag{18}$$

where $\rho = r/P_r$ is the normalised radial variable, and m and n are the indices of Zernike polynomials. One basic fact is that the wavefront aberration after pupil constriction is identical with the original one over the area confined by the smaller pupil size. Based on this equality, a couple of resizing methods have been developed in analytical forms (Schwiegerling 2002, Dai 2006).

In this study, the matrix method proposed by Campbell (2003) is used to resize the measured aberration in the application of dynamic image precompensation. Suppose the pupil radius is reduced from P_r to P_r'. Then, their ratio τ is given by

$$\tau = \frac{P_r'}{P_r} = \frac{\rho'}{\rho}. \tag{19}$$

From the analysis above, it is known that

$$\sum a_n^m Z_n^m(\rho,\theta) = \sum b_n^m Z_n^m(\rho',\theta), \tag{20}$$

where b_n^m is the new set of coefficients that describe the aberration after the pupil size is reduced. After expansion, the equation becomes

$$\sum a_n^m N_n^m R_n^{|m|}(\rho) M(m,\theta) = \sum b_n^m N_n^m R_n^{|m|}(\rho') M(m,\theta). \tag{21}$$

The summation in the last equation can be represented in the form of multiplications of matrices and coefficient vectors. In order to get the analytical solution for b, the Zernike functions Z_n^m are reordered with the double indexing pairs (m,n) in a particularly designed sequence: $(-n_{\max}, n_{\max})$, $(-n_{\max}+1, n_{\max}-1)$, $(-n_{\max}+2, n_{\max}-2) \cdots (n_{\max}-2, n_{\max})$, $(n_{\max}-1, n_{\max}-1)$, $(n_{\max}, n_{\max})$. $n_{\max}$ is the highest order of the Zernike polynomials considered. Following the sequence, the terms of the Zernike functions Z_n^m are decomposed to matrices N, R and M, respectively. This sequence ensures that these matrices are inversable, facilitating the solution for the new coefficients.

Assuming the new coefficient vector b can be obtained through a conversion matrix C, the relationship between the original coefficients vector a and the new coefficient vector b is simply represented as

$$b = Ca. \tag{22}$$

Thus, the matrix representation of Equation (21) is given by

$$TRMNa' = RMNC'a', \tag{23}$$

where a' is the vector of original coefficients with reordered sequence and C' is the conversion matrix for the reordered coefficients. As a diagonal matrix, T is determined by the powers of the ratio τ. R is the radial matrix with the terms of $R_n^{|m|}$. M is the azimuthal matrix with the terms of $M(m,\theta)$ and N is the normalisation matrix with the terms of N_n^m. Thus, C' can be solved by

$$C' = N^{-1}R^{-1}TRN \tag{24}$$

as the terms of M are constants that can be cancelled. Finally, in order to restore the coefficients to the original sequence, a permutation matrix P is introduced to form the conversion matrix:

$$C = P^{\mathrm{T}}N^{-1}R^{-1}TRNP, \tag{25}$$

where P^{T} is the transpose of P. It is important to indicate that the resizing of the ocular aberration is only possible when the new pupil size is smaller than the original. If the new

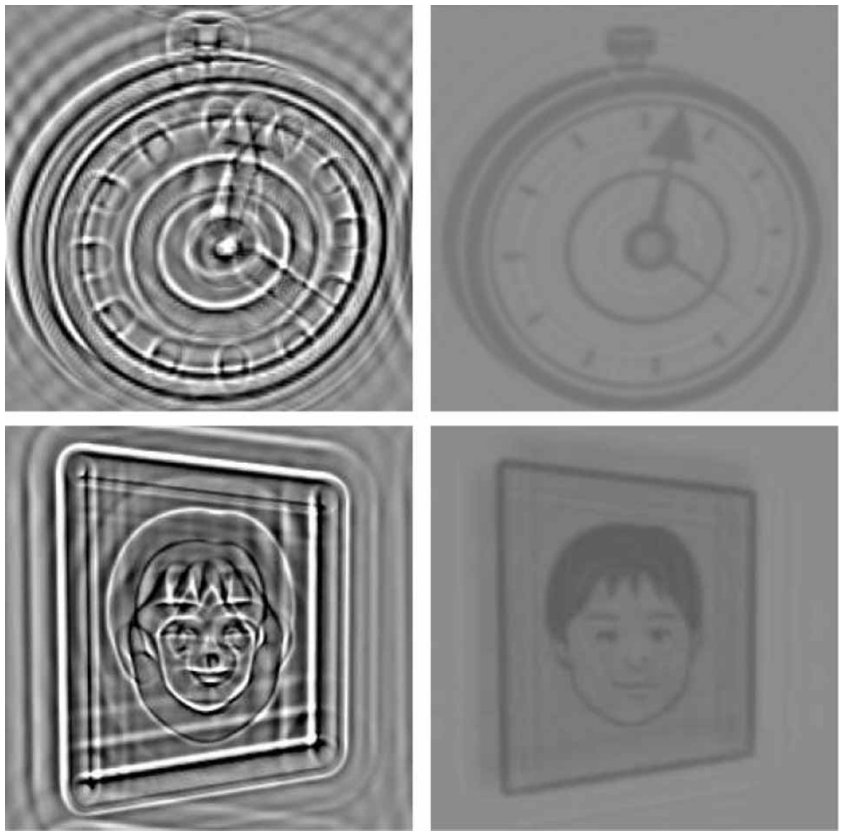

Figure 5. Left column: images with adjusted compensation to pupil diameter 3.5 mm. Right column: retinal images when viewing the images in the left column with pupil diameter 3.5 mm.

pupil size is larger, the aberration data outside the original pupil area will not be available. Thus, there is no accurate and reliable way to resize the aberration to a larger pupil size with unknown information. In this study, this is not a problem since the normal environment of computer use is usually brighter than the environment of aberration measurement, in which the subjects look at a target within a dark chamber.

With this matrix transformation method, the new Zernike coefficients can be easily obtained and used to update the image compensation process. The simulation results in Figure 5 show the images with updated compensation and the retinal images of the viewer, which become clear again with the rematched pupil size of 3.5 mm. It is also found that the retinal images in Figure 5 have less degradation than Figure 2. This is because the aberration of the eye is mitigated as the pupil size reduces.

3.5. Dynamic precompensation

The dynamic nature of ocular aberrations requires the image compensation to be updated dynamically. With the referential Zernike coefficients and pupil size obtained from the wavefront sensor, the new coefficients can be obtained by the resizing of the aberration to a new pupil size, over which the new ocular aberration is reconstructed. Therefore, another requirement of our dynamic precompensation method is that the real-time pupil sizes of the user need to be available during the time of viewing. In this study, the real-time pupil diameters are collected through an eye tracking system. Detailed information of the eye tracking system used will be provided in the next section. Overall, the dynamic precompensation system is demonstrated as a schematic diagram in Figure 6.

4. Experiment

The potential benefit of the dynamic precompensation method has been explored through software simulation. In order to validate the effectiveness of the method, it needs to be tested with real human observers under a realistic environment of computer use. The only reliable way to evaluate the image quality perceived by the observers is to ask their subjective opinions regarding the images. One popular image quality assessment method is asking the subjects to quantify their subjective perception by grades, with or without reference images presented simultaneously (Alpert and Evain 1997, Tang *et al.* 2004). However, with this method, the subjective grades obtained depends highly on the judgement and preference of the subjects.

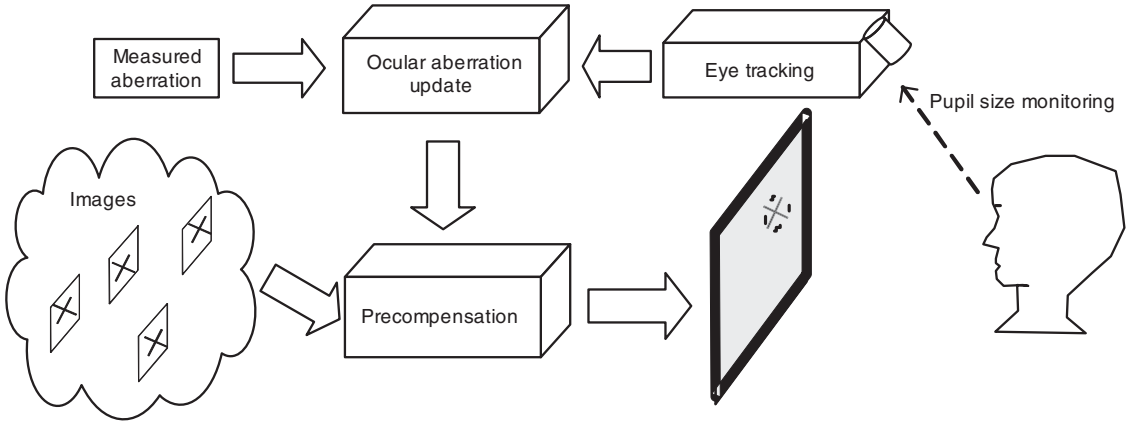

Figure 6. Schematic diagram of the dynamic precompensation system. The image precompensation is updated along with the resized aberration according to the monitored pupil variations.

In this study, an empirical experiment with human participants was conducted to evaluate the benefit of the precompensation method, as a series of image recognition tests. As correct and efficient image recognition is usually the first step of many computer manipulations, image recognition ability is a reasonable indicator of the visual performance of computer users. More importantly, it provides an objective metric to evaluate the visual improvement achieved by the application of the image precompensation.

Besides the recognition accuracy, we were also interested in the subjective impressions of the subjects to the perceived quality of the test images, especially with respect to their perceived sharpness. Thus, as a complement to the quantified recognition accuracy, the subjective impressions to the test images with or without precompensation were collected through a brief questionnaire after the tests.

4.1. Experimental images

The images used in the experiment include 26 English letters and 8 icons. All of the English letters are capital and displayed in Arial font. The eight icons are commonly used by software interfaces, indicating Copy, Document, Folder, Email, Picture, Print, Save and Delete, respectively. These test images are shown in Figure 7. In each test condition, only eight letters were selected from the alphabet at random to be presented.

The canvas size of all test images is 256 × 256 pixels. There are two versions of each test image, with different size of the contents (letter or icon) embedded. The small size version spans 48 × 48 pixels and the large size version spans 72 × 72 pixels. All the test images are black and white without any colour information, making their recognition easier. The canvas of the test images is set to be completely white. When the image precompensation is disabled, the selected image was displayed directly without any processing. Otherwise, the selected image would be compensated based on the subject's ocular aberration that is computed in real time, before presenting it on the screen. Once presented, the image would not be updated until the next image was requested.

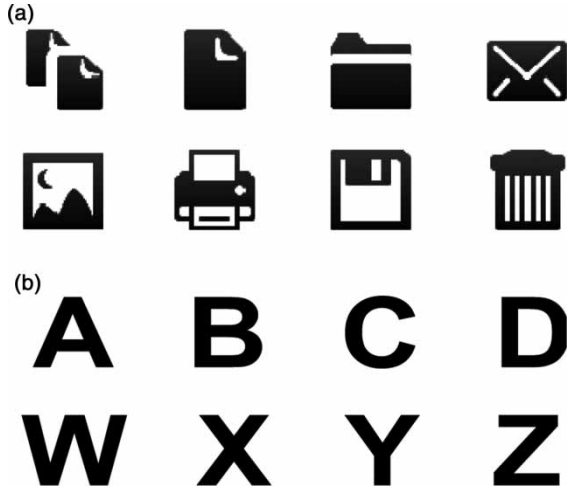

Figure 7. The test images used in the recognition tests: (a) eight icons that indicate Copy, Document, Folder, Email, Picture, Printer, Save and Delete, respectively, from left to right and top to bottom; (b) eight example letters in Arial font (A, B, C, D, W, X, Y, Z). In the tests, the letters displayed were selected randomly from the alphabet.

4.2. Subjects

Twenty human subjects were recruited to participate in our experiment. The age of the subjects ranged from 20 to 33 years (13 male and 7 female). All of them are undergraduate or graduate students, with high degree myopia or astigmatism. The spherical error of the eyes of the participants ranged between −3.24 and −10.34 D and their cylindrical error ranged between −0.22 and −2.44 D. The descriptive statistical information of the subjects is shown in Table 1. All of the subjects performed the tests with both

Table 1. Mean and standard deviation of the ages, spherical and cylindrical error, and measured pupil diameters of the 20 subjects in the experiment.

Age (years)	26.7 ± 3.4
Spherical error (D)	-6.17 ± 1.63
Cylindrical error (D)	-0.88 ± 0.58
Measured pupil diameter (mm)	5.60 ± 0.72

eyes (one eye at a time). Thus, 40 eyes in total were tested in the experiment. An IRB-approved consent form was signed by all of the subjects before the test. During the tests, the subjects were not allowed to wear glasses or contact lenses.

4.3. Experimental setup

The ocular aberration of each subject's eye was initially measured through the Complete Ophthalmic Analysis System (COAS-HD, Wavefront Sciences, Inc), which is based on the Shack–Hartmann wavefront sensing technology. This measurement was conducted only once, since the real-time aberrations were computed by the resizing of the measured aberration data. The COAS-HD is able to measure Zernike coefficients up to 25th order. In this study, we only used Zernike coefficients up to 6th order, represented by 28 terms of the Zernike polynomial. As the referential aberration data of each specific eye, the reported Zernike coefficients, along with the pupil diameter during the measurement, were stored in a separate file.

An eye tracking system (T60, Tobii, Inc) was used to monitor the real-time pupil sizes of each eye, during the viewing phase of the tests. The eye tracker provides pupil diameter measurement at a rate of 60 Hz. The eye tracker is integrated in a 17-inch thin-film-transistor (TFT) computer monitor, which is used as the display device for presenting images in our experiment. The user interfaces of our experiment were developed with Visual C#, including the components that control the presentation sequence and record the recognition performance of the subjects. The data recorded from the subjects were stored in a database for post-analysis.

4.4. Design and procedures

Before the recognition test, each subject was required to take an ocular aberration measurement of their two eyes using the COAS-HD. In order to dilate the pupil of the subject's eyes, the measurement was conducted under dark illumination condition. After the measurement, the subjects were instructed to sit in front of the computer monitor at a distance of 25 inches (0.64 m). The field of view to the test image is approximately 6° in both the vertical and horizontal dimensions. Since the aberration in each eye of an individual are generally different, the recognition tests were based on the monocular vision of the subjects and the image precompensation was designed for only one eye (left or right) at a time. Thus, one eye would be covered by an eye patch while the other eye was viewing the images presented during the test. The tests were performed under office lighting condition, thereby ensuring the pupil sizes would not be larger than the initial one, which was recorded while the aberration was measured.

During the tests, the test images were presented to the subject one by one. The presentation of the images was grouped by the combination of content size (small or large), content category (letter or icon) and use of precompensation (yes or no). Within each group, the presentation sequence of test images was randomised. Moreover, the order of groups to be presented was also randomised. Each test image selected with or without precompensation was presented only once for each eye. The original test images were presented before or after the test images with precompensation and their internal sequence order was also random. As 8 test images were presented in each group, there were

$$8 \times 2(\text{category}) \times 2(\text{size}) \times 2(\text{method}) = 64 \qquad (26)$$

trials in total for each eye. In each trial, the subject was asked to identify the presented image verbally. Based on the answer, the recognition trial was recorded as correct or incorrect. The test images were presented on the screen for only 3 s. After that, the current test images would be hidden. This helped to promote the spontaneity of the subject's answers. After completing the tests of one eye, the subject was allowed to take a 5 min break before doing the tests of the other eye.

In this study, the empirical experiment used a factorial design that had three factors: image category, with two levels (icon or letter), content size, with two levels (small and large), and use of image precompensation, with two levels (yes or no). The dependent variable was the number of correct recognitions made by the subjects in each condition, ranging from 0 to 8. The experimental data were analysed through a three-way ANOVA with repeated measures to evaluate the effects of our dynamic precompensation method. The evaluation was based on the recognition accuracy achieved by the subjects. The interactions between precompensation method and other factors were also investigated.

4.5. Results

From the analysis, it was found that the effect of precompensation on the recognition accuracy was significant, $F(1, 39) = 70.02, p < 0.01$. With the dynamic image precompensation, the mean of correct recognitions increased from 3.86 to 5.88. That is, the average accuracy ratio increased from 48.3% to 73.5%. This indicates that the visual performance of the subjects was significantly improved when the test images were compensated before presenting them on the screen, even though there were still

some images that could not be identified correctly. Considering the fact that the test images were presented for only 3 s, the improvement achieved was quite encouraging. As we expected, the effect of content size of the test image on the recognition accuracy was significant, $F(1, 39) = 185.9$, $p < 0.01$. The reason for this significance is quite intuitive, since recognition of large letters or icons was less impeded by the degradation than the recognition of small ones. The means of correct recognitions for different groups of images are shown in Figure 8.

The interaction between the content size of the image and the precompensation was found to be significant, $F(1, 39) = 10.57$, $p < 0.01$. This reflects that the recognition accuracy improvement for the images with large letters or icons was not as marked as for the small ones when the precompensation was applied. This can be explained by the fact that letters and icons of large size could be recognised correctly by most of the subjects, even if presented without precompensation. More interestingly, the interaction between the content category and the precompensation was also found to be significant, $F(1, 39) = 21.37$, $p < 0.01$. From the analysis, we found that the accuracy improvement for the icons was lower than for the letters after the precompensation was applied. This is probably because the icons were more vulnerable to the ringing artefacts introduced in the process of precompensation, as the test icons generally had more complicated shapes than the letters.

After the tests, subjective impressions to the test images were collected. The participants were requested to give their answers based on their impressions of the test images during the tests. The test images presented with precompensation were easily distinguished by the subjects from the original ones due to their darker background. Consistent with the improvement reflected on the recognition accuracy, most of the subjects (18 of 20) reported that the sharpness of the test images was increased after precompensation was applied. Interestingly, most of the subjects (17 of 20) believed that the images with letters were more easily identified than the icons.

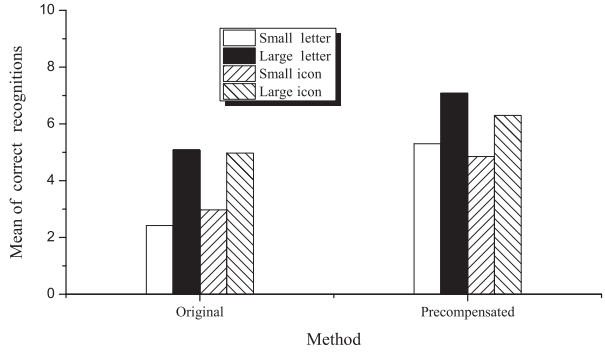

Figure 8. Average correct recognitions made by the subjects to the images of different groups with small letters, large letters, small icons and large icons.

5. Discussion

Aside from the recognition performance, pupil variations of each eye during the tests were also recorded. The recorded pupil data contain the exact pupil diameter used to resize the wavefront aberration of the eye in each trial of the test. Figure 9 shows a typical example of recorded pupil diameters during the tests. It was observed that some pupils constricted much more than others compared with the measured pupil diameters corresponding to the original aberration data. It was also speculated that the process of resizing the ocular aberration to the constricted size might introduce extra degradation into the precompensated image. To explore this conjecture, we investigated the relationship between the average deviations of the pupil size from the initial value and the improvement of correct recognitions achieved by the 40 eyes that were tested in the experiment, as shown in Figure 10. From the analysis, we found no significant correlation between the root mean square (RMS) of the average pupil size deviations and the average increase of correct recognition number, $p > 0.05$. This indicates that the performance of the method was not diminished when larger adjustment of the ocular aberration was needed.

Thus, the limitation of the precompensation method mainly comes from the process of inverse Wiener filtering. The ringing artefacts and noise amplification are two prevalent problems suffered by the image restoration process (Banham and Katsaggelos 1997). The former is caused by the regularisation error distributed on the whole spectrum, usually becoming evident around the regions with abrupt intensity transitions. The latter may cause extra degradation to the restored image depending on its scale. Similar to the image restoration problem, the image precompensation method is also subject to these two challenges. The noise in image precompensation is primarily from the aberration measurement and the display devices. The pollution caused by noise amplification may not be so critical since the amplified high-frequency components will be attenuated by the

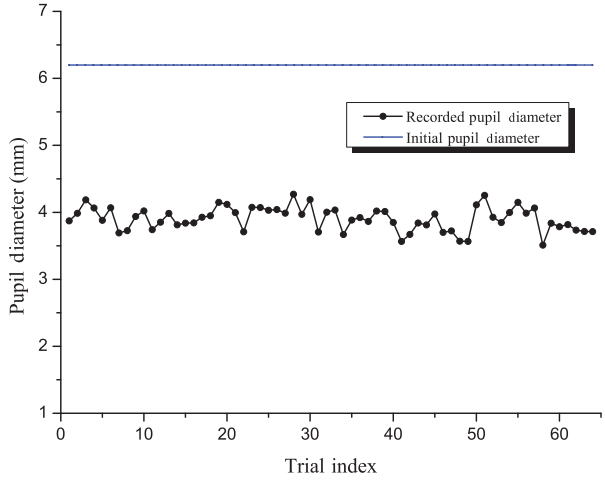

Figure 9. One typical example of pupil variations recorded in the tests.

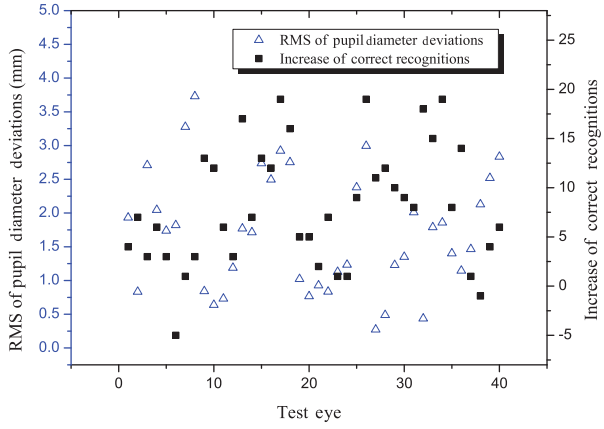

Figure 10. RMS of the average deviations from the initial pupil diameters and the average increase of the correct recognitions for each test eye when the precompensation was applied. No significant correlation was found between them and the covariance coefficient is −0.005 that is close to zero.

eye during the viewing process. In other words, people with ocular aberration may not be able to perceive the amplified high-frequency noise when viewing the compensated image due to the low-pass nature of most ocular aberrations. The biggest new challenge that emerges for image precompensation is the evident contrast reduction observed. Even though we have demonstrated that the essential reason for it is the intensity downscaling of the compensated image for display on a device, it is found that the contrast enhancement is in some extent conflicted with the lessening of ringing artefacts. If the regularisation parameter of the inverse Wiener filter is decreased, the ringing artefacts are relieved, but the contrast of the compensated image becomes even lower. This makes preserving the original contrast without conspicuous artefacts very challenging. Thus, exploring other compensation algorithms that may allow the decoupling of these two phenomena can greatly improve the performance of precompensation. However, our experience, so far, seems to indicate that these two problems are intrinsically coupled. If this is the case, then more practical approach will be to restrict both problems within acceptable levels.

The dynamic precompensation method proposed in this study is designed to overcome the visual blurring caused by the optical aberrations of the eyes. In practice, the image perception quality of the human eye depends not only on the optical aberrations, but also on the neural factors involved in the vision system (Wandell 1995, Good *et al.* 2001). Thus, while theoretically the image precompensation method can be used to counteract any ocular aberrations, it may not benefit the users with retinal and neurological visual problems.

6. Conclusion

In this paper, a dynamic image precompensation method was proposed to improve the visual performance of computer users with ocular aberrations. Personalised precompensation is applied on the images before presenting, to counteract the visual blurring caused by the user's ocular aberration. In order to overcome the problem of static precompensation, the applied compensation is generated based on the dynamic ocular aberration of the eye, which is derived from the initial aberration data measured by wavefront sensors.

The precompensation method has low computation cost and can be set up on any regular personal computers and display devices. Thus, it is possible to implement the real-time precompensation for practical application. In addition, the precompensation method is automated and parameterless, without manual intervention in the application.

The effectiveness of this method was evaluated through the recognition of test images with randomly selected letters and icons. The recognition accuracy of the subjects increased after the method was applied and most subjects reported that sharper images were perceived with the precompensation. The encouraging results from the experiment suggest that the proposed method is a promising way to relieve visual blurring in the human–computer interactions, without using optical devices. Further benefit of the dynamic precompensation method is mainly impeded by the contrast loss problem, which is caused by the presenting of precompensated images with intensity ranges that are beyond the display device's capacity.

References

Alonso, M., *et al.*, 2005. Image pre-compensation to facilitate computer access for users with refractive errors. *Behaviour & Information Technology*, 24 (3), 161–173.

Alpert, T. and Evain, J., 1997. Subjective quality evaluation: the SSCQE and DSCQE methodologies. *EBU Technical Review*, 271, 12–20.

Banham, M.R. and Katsaggelos, A.K., 1997. Digital image restoration. *IEEE Signal Processing Magazine*, 14 (2), 24–41.

Campbell, C.E., 2003. Matrix method to find a new set of Zernike coefficients from an original set when the aperture radius is changed. *Journal of the Optical Society of America A*, 20 (2), 209–217.

Charman, W. and Heron, G., 1988. Fluctuations in accommodation: a review. *Ophthalmic and Physiological Optics*, 8 (2), 153–164.

Dai, G., 2006. Scaling Zernike expansion coefficients to smaller pupil sizes: a simpler formula. *Journal of the Optical Society of America A*, 23 (3), 539–543.

Dai, G., 2008. *Wavefront optics for vision correction*. Bellingham, WA: SPIE Press.

Fernández, E.J., Iglesias, I., and Artal, P., 2001. Closed-loop adaptive optics in the human eye. *Optics Letters*, 26 (10), 746–748.

Fine, E.M. and Peli, E., 1995. Enhancement of text for the visually impaired. *Journal of the Optical Society of America A*, 12 (7), 1439–1447.

Gonzalez, R.C. and Woods, R.E., 2002. *Digital image processing*. Second Prentice Hall.

Good, W.V., *et al.*, 2001. Recent advances in cortical visual impairment. *Developmental Medicine & Child Neurology*, 43 (1), 56–60.

Goodman, J., 2005. *Introduction to Fourier optics*. Englewood, CO: Roberts and Company.

Guirao, A., *et al.*, 2002. Calculated impact of higher-order monochromatic aberrations on retinal image quality in a population of human eyes. *Journal of the Optical Society of America A*, 19 (1), 1–9.

Hofer, H., *et al.*, 2001. Dynamics of the eye's wave aberration. *Journal of the Optical Society of America A*, 18 (3), 497–506.

Huang, J., *et al.*, 2012. Contrast improvement in pre-compensation of ocular aberrations for computer users. *Biomedical Sciences Instrumentation*, 48, 179–186.

Iskander, D.R., *et al.*, 2004. Analyzing the dynamic wavefront aberrations in the human eye. *IEEE Transactions on Biomedical Engineering*, 51 (11), 1969–1980.

Katsaggelos, A.K., *et al.*, 1991. A regularized iterative image restoration algorithm. *IEEE Transactions on Signal Processing*, 39 (4), 914–929.

Kim, J., Vora, A., and Peli, E., 2004. MPEG-based image enhancement for the visually impaired. *Optical Engineering*, 43 (6), 1318–1328.

Lawton, T.B., 1992. Image enhancement filters significantly improve reading performance for low vision observers. *Ophthalmic and Physiological Optics*, 12 (2), 193–200.

Lawton, T.A., *et al.*, 1998. Image enhancement improves reading performance in age-related macular degeneration patients. *Vision Research*, 38 (1), 153–162.

Leat, S.J., *et al.*, 2005. Generic and customised digital image enhancement filters for the visually impaired. *Vision Research*, 45 (15), 1991–2007.

Leonard, R.M., 2001. *Statistics on vision impairment: a resource manual*. 4th ed. New York: Research Institute, Lighthouse International.

Liang, J. and Williams, D.R., 1997. Aberrations and retinal image quality of the normal human eye. *Journal of the Optical Society of America A*, 14 (11), 2873–2883.

Liang, J., Williams, D.R., and Miller, D.T., 1997. Supernormal vision and high-resolution retinal imaging through adaptive optics. *Journal of the Optical Society of America A*, 14 (11), 2884–2892.

Muma, M., Iskander, D.R., and Collins, M.J., 2010. The role of cardiopulmonary signals in the dynamics of the eye's wavefront aberrations. *IEEE Transactions on Biomedical Engineering*, 57 (2), 373–383.

Munoz, B., *et al.*, 2000. Causes of blindness and visual impairment in a population of older Americans: The Salisbury Eye Evaluation Study. *Archives of Ophthalmology*, 118 (6), 819–825.

Peli, E., 1984. Image enhancement for the visually impaired. *Optical Engineering*, 23 (1), 47–51.

Peli, E., 2005. Recognition performance and perceived quality of video enhanced for the visually impaired. *Ophthalmic and Physiological Optics*, 25 (6), 543–555.

Peli, E., *et al.*, 1994. Image enhancement for the visually impaired: the effects of enhancement on face recognition. *Journal of the Optical Society of America A*, 11 (7), 1929–1939.

Peli, E., *et al.*, 2004. Wideband enhancement of television images for people with visual impairments. *Journal of the Optical Society of America A*, 21 (6), 937–950.

Richardson, W.H., 1972. Bayesian-based iterative method of image restoration. *Journal of the Optical Society of America*, 62 (1), 55–59.

Roorda, A., 2011. Adaptive optics for studying visual function: a comprehensive review. *Journal of Vision*, 11 (5), 1–21.

Rudin, L.I., Osher, S., and Fatemi, E., 1992. Nonlinear total variation based noise removal algorithms. *Physica D: Nonlinear Phenomena*, 60 (1–4), 259–268.

Sawides, L., *et al.*, 2010. Visual performance with real-life tasks under adaptive-optics ocular aberration correction. *Journal of Vision*, 10 (5), 1–12.

Schwiegerling, J., 2002. Scaling Zernike expansion coefficients to different pupil sizes. *Journal of the Optical Society of America A*, 19 (10), 1937–1945.

Tang, J., Kim, J., and Peli, E., 2004. Image enhancement in the JPEG domain for people with vision impairment. *IEEE Transactions on Biomedical Engineering*, 51 (11), 2013–2023.

The Eye Diseases Prevalence Research Group, 2004. The prevalence of refractive errors among adults in the United States, Western Europe, and Australia. *Archives of Ophthalmology*, 122, 495–505.

Thibos, L., 2000. Formation and sampling of the retinal image. *In*: K.K.D. Valiois, ed. *Seeing*. 2nd ed. San Diego, CA: Academic Press, 1–54.

Vitale, S., Sperduto, R.D., and Ferris III, F.L., 2009. Increased prevalence of myopia in the United States between 1971–1972 and 1999–2004. *Archives of Ophthalmology*, 127 (12), 1632–1639.

Wandell, B.A., 1995. *Foundations of vision*. Vol. 93. Sunderland, MA: Sinauer Associates.

Winn, B., *et al.*, 1994. Factors affecting light-adapted pupil size in normal human subjects. *Investigative Ophthalmology & Visual Science*, 35 (3), 1132–1137.

Wolffsohn, J.S., Mukhopadhyay, D., and Rubinstein, M., 2007. Image enhancement of real-time television to benefit the visually impaired. *American Journal of Ophthalmology*, 144 (3), 436–440.

Copyright of Behaviour & Information Technology is the property of Taylor & Francis Ltd and its content may not be copied or emailed to multiple sites or posted to a listserv without the copyright holder's express written permission. However, users may print, download, or email articles for individual use.